ELSEVIER

Materials Science and Engineering A349 (2003) 236–247

MATERIALS SCIENCE & ENGINEERING A

www.elsevier.com/locate/msea

# The microstructure and the thermal expansion characteristics of $Cu/SiC_p$ composites

Kuen-Ming Shu *, G.C. Tu

*Department of Materials Science and Engineering, National Chiao-Tung University, 1001 Ta Hsueh Road, Hsinchu 30050, Taiwan, ROC*

Received 14 June 2002; received in revised form 30 September 2002

**Abstract**

Copper/silicon carbide composites ($Cu/SiC_p$) were made by the powder metallurgy method. Electroless plating was employed to deposit a copper film on $SiC_p$ powder before mixing with Cu powder in order to improve the bonding status between Cu and SiC particles during sintering. Thermal expansion property of as-formed product was measured in the temperature range from 50 to 550 °C. The results showed that copper coating on silicon carbide particles could render uniform distribution of $SiC_p$ in the copper matrix. The composites exhibited positive thermal hysteresis behavior when cooled down from the peak temperature to room temperature, which can be explained in terms of the residual stresses and the interfacial bonding between copper and silicon carbide. The magnitude of this strain was a function of the $SiC_p$ volume fraction and the number of thermal cycles. The thermal expansion property of composites was measured and compared with those predicted from various theoretical models.
© 2002 Published by Elsevier Science B.V.

*Keywords:* Powder metallurgy; Electroless plating; $Cu/SiC_p$ composites; Microstructure; Coefficient of thermal expansion; Thermal hysteresis strain

## 1. Introduction

Metal matrix composites (MMC) are rapidly becoming prime candidates as structural material in engineering application. For example, aluminum reinforced by $Al_2O_3$ and $SiO_2$ is used in the aerospace, aircraft and automotive industries because of its excellent thermophysical properties such as low coefficient of thermal expansion (CTE), high thermal conductivity, and improved mechanical properties such as higher specific strength, better wear resistance, and specific modulus. Recently, metal–ceramic composites with high ceramic contents have become another focus for thermal management applications such as electronic packaging [1–5]. The widespread use of these composites requires a deep understanding of their thermal expansion and some relative properties. For instance, the packaging materials in microelectronics should have high thermal conductivity to dissipate the heat, and low CTE to decrease the thermal expansion mismatch among the devices.

Low and suitable CTE, together with good thermal conductivity, can be achieved by blending appropriate metallic and ceramic phases to form a composite. Despite many theoretical and experimental studies [6–10] having been carried out on the subject of CTE of particle-reinforced MMC, few of them are directed toward the effect of particle surface coating on the thermal expansion behavior and other characteristics of these composites. It was thus considered worthwhile to fabricate the copper-based ceramic-reinforced composites and to study their thermal expansion characteristics, in which the ceramic particles were pre-coated with copper film through an electroless plating process before mixing.

## 2. Experimental procedure

The reinforcements used in the present work were angular-shaped silicone carbide particles ($SiC_p$) with nominal diameters of 5, 25 and 47 μm. The SiC particles are available in hexagonal ($\alpha$) and cubic ($\beta$) crystal

* Corresponding author. Tel.: +86-65-632-9643; fax: +88-65-631-0824.
*E-mail address:* kmshu@sunws.nhit.edu.tw (K.-M. Shu).

0921-5093/02/$ - see front matter © 2002 Published by Elsevier Science B.V.
PII: S0921-5093(02)00788-8

structures from inexpensive raw material sources. They have low density, low CTE, high Young's modulus, and a commercially available particle size range of 1–50 μm. Electrolytic copper powder (99.7% purity) which assume dendritic shape with average particle size of 16 μm was used in this experiment. Table 1 shows the typical properties of $SiC_p$ and Cu. The morphology of both particles are shown in Fig. 1(a) and (b).

In order to obtain optimal bonding between ceramic particles and Cu particles through a completely continuous copper film on $SiC_p$, the following electroless plating steps were applied:

1) Surface treatment: Surface cleaning of $SiC_p$ was accomplished by immersing in acetone under ultrasonic vibration for 30 min. After rinsing with deionized water, $SiC_p$ were heated at 600 °C for 3 h in an air drying oven, and were subsequently ground to break agglomerated particles.
2) Sensitizing and activating: The cleaned $SiC_p$ were sensitized in a solution containing stannous chloride ($SnCl_2 \cdot 2H_2O$) and hydrochloric acid (HCl) for an hour and then activated in a solution containing palladium chloride ($PdCl_2$) and hydrochloric acid for an hour.
3) Electroless copper plating process: The cleaned and activated $SiC_p$ (60 g $l^{-1}$) were placed separately into $CuSO_4 \cdot 5H_2O$ (20 g $l^{-1}$) and $KNaC_4H_4O_6$ (50 g $l^{-1}$) solutions, ultrasonically shaken, followed with continuous stirring during mixing of the two solutions. Then, HCOH (36%) solution was added to the mixed solution. The pH of the solution was subsequently adjusted by adding NaOH to pH 13; at this stage, copper started to plate onto $SiC_p$ surface.

The copper content was determined by dissolving the plated copper film on $SiC_p$ in nitric acid, and the measured copper film percent on $SiC_p$ was 7±0.5 wt.% in this experiment.

Copper coated $SiC_p$ was combined with adequate copper powders to obtain the following Cu/$SiC_p$ mixes

Table 1
Typical properties of $SiC_p$ and Cu

| Property | Value | Materials | |
|---|---|---|---|
| | | $SiC_p$ | Cu |
| Density | g $cm^{-3}$ | 3.20–3.26 | 8.96 |
| Young's modulus | GPa | 400–500 | 110 |
| Melting temperature | °C | 2600 | 1083 |
| Tensile strength | GPa | > 3.2 | 0.20–0.24 |
| CTE | $10^{-6}$ $K^{-1}$ | 5.40 | 16.5 |
| Poisson's ratio | | 0.17 | 0.33 |
| Shear modulus | GPa | 175 | 48.3 |
| Thermal conductivity | W $m^{-1}$ $K^{-1}$ | 120 | 392 |

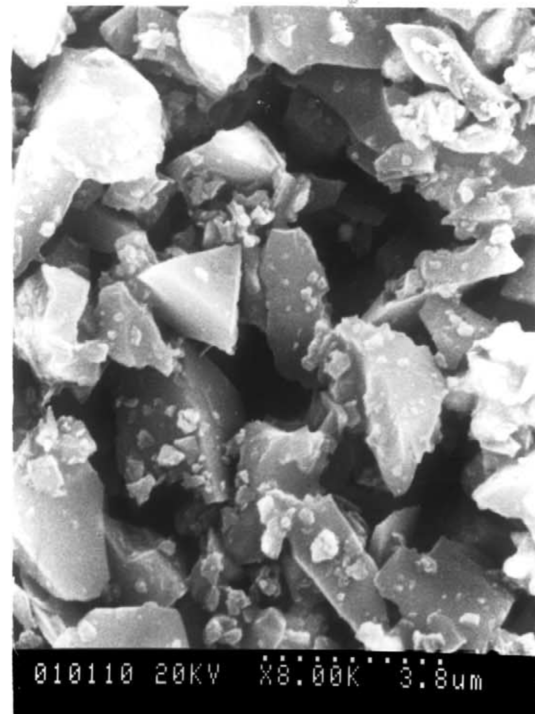

(a)

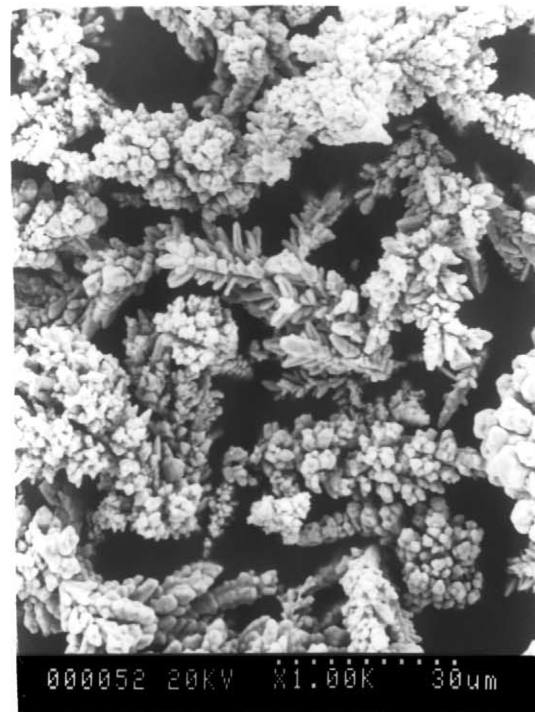

(b)

Fig. 1. The morphology of as-received powders: (a) $SiC_p$, and (b) Cu.

with weight ratios of 1:1, 2:1, 3:1, 4:1 and 5:1, which corresponding to 74, 58, 48, 41 and 35 vol.% $SiC_p$, respectively. Then these powders were dry mixed for 4 h using Turbula® 3-D mixer in argon atmosphere. The resulting powders were filled into a steel mold of 8 mm

diameter, and then a pressure of 760 MPa was applied and maintained for 180 s to form a cylindrical green compact. The green compact was sintered at 850 °C in nitrogen for 8 h and then cold repressed in a steel mold of 8.1 mm diameter at a pressure of 1140 MPa for 10 min. Both end surfaces of repressed compacts were finally polished by #2000 sandpaper for CTE test.

True densities of the composites were measured by using the buoyancy (Archimedes') method (ASTM B328) and compared with theoretical densities to obtain varying degree of densification.

The CTE at a particular temperature can be derived using the relationship:

$$\mathrm{CTE} = \frac{\partial}{\partial T}\left(\frac{\Delta L}{L}\right) \quad (1)$$

where $L$ is the length of the specimen at temperature $T$.

The mean linear CTE ($\overline{\mathrm{CTE}}$) was calculated by the formula:

$$\overline{\mathrm{CTE}} = \frac{1}{L_0}\left(\frac{\Delta L}{\Delta T}\right) \quad (2)$$

where $L_0$ is the original length of the specimen and $\Delta L$ is the change in length over a temperature interval $\Delta T$.

The measurements of CTE and $\overline{\mathrm{CTE}}$ of the specimens were performed on a Thermal Analyst 2100 thermal mechanical analyzer using inbuilt software, over a temperature range from 50 to 550 °C at heating and cooling rates of 15 °C min$^{-1}$ in the atmosphere of argon. Three specimens were tested for each condition, and the average data were adopted for analysis. The metallography of the product was accomplished using an optical microscope and a scanning electron microscope.

## 3. Results and discussion

### 3.1. Distribution of $SiC_p$

The cross-section microstructure of the Cu-coated $SiC_p$ powder is shown in Fig. 2, and this shows that the coated copper film was homogeneous and continuous. The results of X-ray diffraction analysis on $SiC_p$ coated with copper film are shown in Fig. 3, both Cu and SiC were detected, indicating the presence of copper film on the $SiC_p$ surface. Representative micrographs of the fracture surface of the composite with 35 vol.% $SiC_p$ are given in Fig. 4(a) and (b). It can be seen from Fig. 4(a) that the non-coated $SiC_p$ in the composite appeared angular in shape, and bad bonding existed between the Cu matrix and the non-coated $SiC_p$. In Fig. 4(b), the copper film on the $SiC_p$ particle surface is still observed on the fracture surface, and there was better bonding status between the Cu matrix and the $SiC_p$ particles. The fracture surfaces of both specimens exhibit plastic behavior, the fracture is ductile showing extensive dimple formation on the fracture surface, the major dimples can be observed with SiC particles embedded in them.

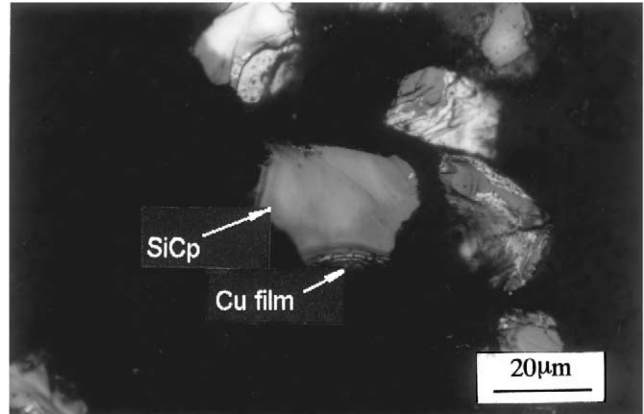


Fig. 2. Cross-section microstructure of the Cu-coated $SiC_p$ composite powders.

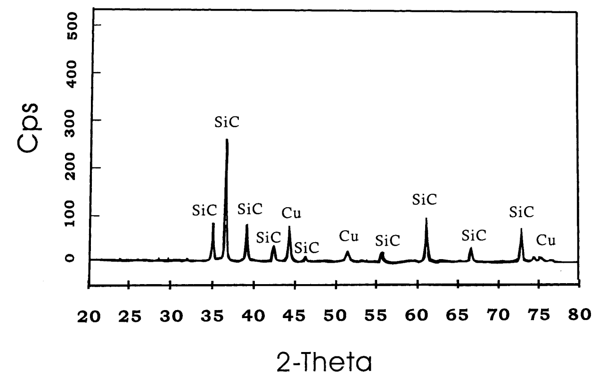


Fig. 3. The X-ray diffraction of Cu-coated $SiC_p$ particles.

Optical microstructures of several Cu/$SiC_p$ composites are shown in Fig. 5(a) and (b). It can be seen from Fig. 5(a) that the non-coated $SiC_p$ in the composite appeared more clustering phenomena and the reinforcement touching one another when the $SiC_p$ concentration is up to 35 vol.%. While in Fig. 5(b), for Cu-coated $SiC_p$, particles are distributed uniformly in the Cu matrix, and good bonding status appeared between copper and $SiC_p$. This status is required in order to achieve effective load transfer from the matrix to the reinforcement.

Considering the role of phase continuity in determining the properties of the composite, three extreme cases are shown in Fig. 6. Fig. 6(a) shows the arrangement that individual $SiC_p$ particles are dispersed in continuous Cu matrix; this model is henceforth referred as continuous ductile phase model [11]. The Cu/$SiC_p$ composite with 35 vol.% Cu-coated $SiC_p$, as shown in Fig. 5(b), belongs to this model. When $SiC_p$ concentration exceed approximately 0.5, the majority of the

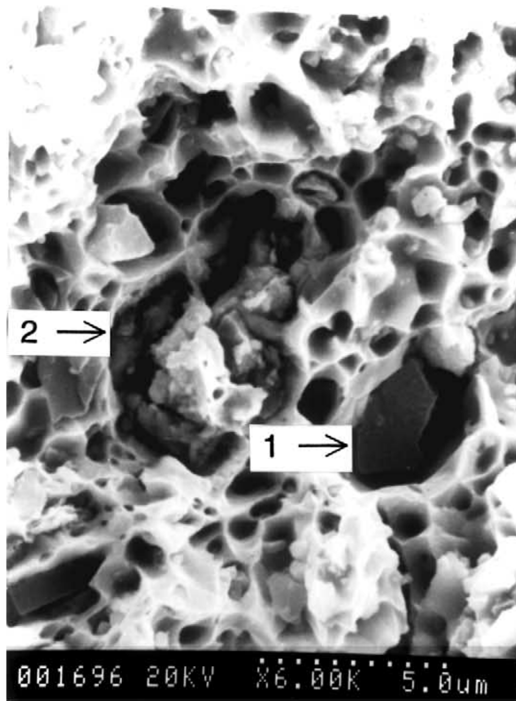


(a)

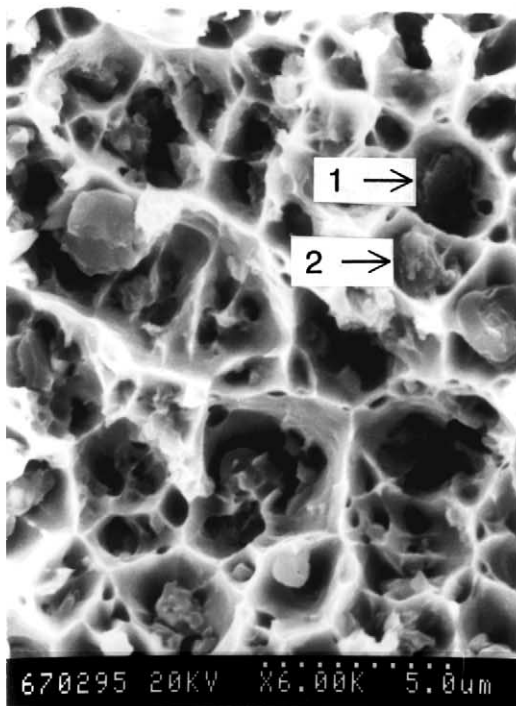


(b)

Fig. 4. The micrographs of the fracture surfaces: (a) non-coated sample, 1 is decohesion of $SiC_p$/Cu interface, 2 is $SiC_p$ cracked by pressing or tensile test. (b) Copper coated electrode, 1 is cracked $SiC_p$, 2 is copper coated $SiC_p$.

particles can begin to touch one another, here, a continuous dispersion of $SiC_p$ particles encompasses

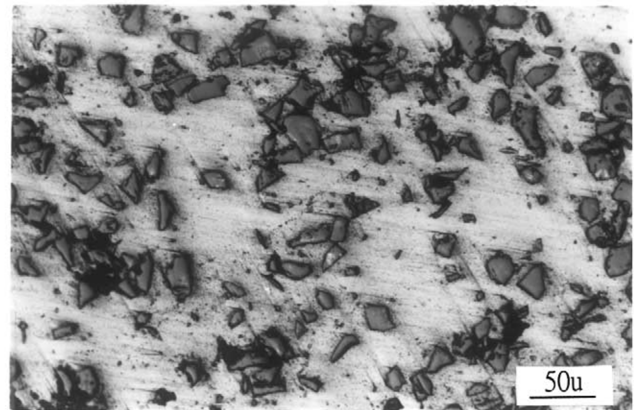


(a)

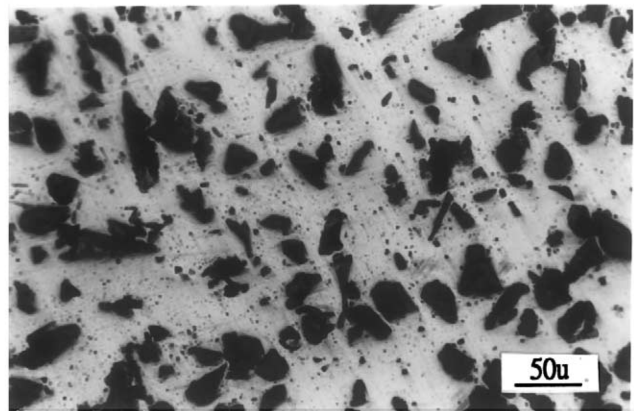


(b)

Fig. 5. Optical micrographs showing the microstructure of Cu/$SiC_p$ composites: (a) 35 vol.% 25 μm $SiC_p$, non-coated, (b) 35 vol.% 47 μm $SiC_p$, Cu-coated.

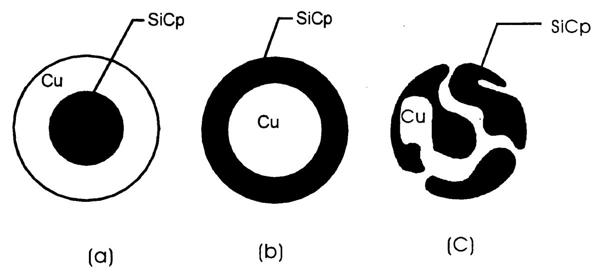


Fig. 6. Schematic diagrams showing three models with different phase configurations: (a) continuous ductile phase model [11], (b) continuous brittle phase model [11], (c) interpenetrating model.

islands of ductile Cu phase. Fig. 6(b) shows the unit cell for this continuous brittle phase model, these kind composites are classified as ceramic matrix composite. But, the Cu/$SiC_p$ composite with 35 vol.% non-coated $SiC_p$, as shown in Fig. 5(a), some Cu and $SiC_p$ are entangled and touched each other, this kind model is referred as interpenetrating model, as shown in Fig. 6(c). When the composites are classified as continuous ductile phase model, it can be imaged, owing to the difference

of CTE value of Cu and $SiC_p$, the space volume occupied by $SiC_p$ in copper matrix will expanded larger than $SiC_p$ volume expansion when temperature increases. Copper would dominate the composite CTE while there is no bonding force at the interface to restrict copper expansion. On the contrary, both Cu and $SiC_p$ would dominate the composite CTE if good bonding exists at the interface. Under continuous brittle model situation, the space volume occupied by copper particle expands less than copper volume expansion; in this case, even poor bonding exists at the Cu/$SiC_p$ interface, both Cu and $SiC_p$ dominate the composite CTE. As in the present study, this brittle model is rarely occurred in reality, due to the brittleness and the shape of reinforcement particle. In the case of interpenetrating model, copper would dominate composite CTE when no bonding exists at the interface. However, the CTE would be dominated by both Cu and $SiC_p$ since $SiC_p$ restricted copper expansion in case that good bonding exists at the interface.

### *3.2. Sintered density and porosity*

The true densities of sintered and repressed specimens obtained by Archimedes' law and the theoretical values are given in Table 2. It shows that the density of the composite decreases as the amount of $SiC_p$ increases, and when the particle size increases. Because of the less-bonding status between $SiC_p$ and Cu, the composite density of non-coated $SiC_p$ is lower than that of Cu-coated $SiC_p$.

In the ceramic reinforced MMC system, the less-bonding characteristic between metal and ceramic, interfacial energy is required to enhance or induce the bonding between metal and ceramic even in liquid phase sintering. Composites fabricated by the coating method do not have such a requirement and can be compacted to higher densities. In composite with low $SiC_p$ volume fraction, less Cu/$SiC_p$ interface means less copper atom diffusion barrier, copper atoms can diffuse readily and fill the interstices between the $SiC_p$, thus leading to a higher densification of the composites.

For comparison, pure copper powder with the same procedures to fabricate P/Med copper, was also prepared and tested, and a higher than 96% of the theoretical density was obtained.

Porosity gives the fraction of the total void volume, which can be determined by the equation [12]:

$$p_f = 1 - \frac{\rho}{\rho_0} \tag{3}$$

where $p_f$ is the pore volume fraction, $\rho$ the measured density, and $\rho_0$ the theoretical density.

Fig. 7 shows the porosity as a function of vol.% $SiC_p$ for various-processed composites, it apparently reveals that the porosity of all composites increased markedly with increasing $SiC_p$ volume fraction. For the composite made by the coated copper method, the porosity remained lower than that made by the non-coated $SiC_p$ even at higher $SiC_p$ volume fraction such as 74 vol.% $SiC_p$.

### *3.3. Influence of particle size on CTE of the composite*

Of the possible thermal behavior characteristics, the behavior of thermal expansion of MMCs has been one of the most extensively studied, since it effects the mechanical behavior of the composites in severe thermal environment, especially the application of composites in engine components and space structures. The stability of MMCs over a long period of time becomes the critical design consideration. The stability can be described in two aspects, geometrical changes and mechanical property changes. In the former case the CTE of the MMC plays a key role, while in the latter case the mismatch of CTEs between the metal matrix and particles has a dominant effect.

The currently available $SiC_p$ particles generally exhibit a Young's modulus of 450 GPa and a CTE of about $5.40 \times 10^{-6}$ $K^{-1}$ , while the compared values of copper are 110 GPa and $16.5 \times 10^{-6}$ $K^{-1}$ (20–300 °C) for young's modulus and CTE, respectively, [13,14]. Therefore, it is expected that the CTE of the composite will be lowered with the addition of $SiC_p$ volume fraction. Table 3 shows the instantaneous and mean CTE of all specimens in this experiment during first cycle heating stage. It can be observed that within the entire temperature range investigated, the CTE values increase apparently with increasing $SiC_p$ size and decrease with increasing $SiC_p$ volume fraction.

The mismatch of the CTE values between the reinforcement and the matrix causes the stress in the matrix, as was reported by Masutti et al. [15]. The thermal stresses arising in the matrix could possibly exceed the yield stress of the copper matrix at a particular temperature, thus resulting in plastic deformation in the matrix. A mechanism is proposed to determine the relationship between thermal stress and particle size.

Assuming the particle to be spherical, according to Brooksbank et al. [16] and Vaidya et al. [17], the particle was surrounded by a spherical shell of the matrix, as shown in Fig. 8 .The radial and circumferential stress in the matrix can be expressed as:

$$\sigma_{rm} = \frac{p[(a^3/r^3) - V_p]}{1 - V_p} \tag{4}$$

$$\sigma_{\theta m} = \frac{p[0.5(a^3/r^3) + V_p]}{1 - V_p} \tag{5}$$

Table 2
Density of sintered and repressed samples

| Particle size (μm) | $SiC_p$ | | | | | | | | | | | | | | |
|---|---|---|---|---|---|---|---|---|---|---|---|---|---|---|---|
| | 35 vol.% | | | 41 vol.% | | | 48 vol.% | | | 58 vol.% | | | 74 vol.% | | |
| | Coated | Non-coated | Theoretical | Coated | Non-coated | Theoretical | Coated | Non-coated | Theoretical | Coated | Non-coated | Theoretical | Coated | Non-coated | Theoretical |
| 5 | 7.34 | 7.01 | 7.71 | 7.04 | 6.74 | 7.48 | 6.64 | 6.36 | 7.15 | 6.00 | 5.83 | 6.61 | 4.98 | 4.88 | 5.63 |
| 25 | 7.04 | 6.98 | 7.71 | 6.68 | 6.50 | 7.48 | 6.35 | 6.21 | 7.15 | 5.83 | 5.74 | 6.61 | 4.94 | 4.87 | 5.63 |
| 47 | 6.95 | 6.86 | 7.71 | 6.52 | 6.43 | 7.48 | 6.23 | 6.15 | 7.15 | 5.75 | 5.63 | 6.61 | 4.82 | 4.71 | 5.63 |

$$p = \frac{(\alpha_m - \alpha_p)\Delta T}{[0.5(1+\nu_m) + (1+2\nu_m)/E_m(1-V_p)] + [V_p(1-2\nu_p)/E_p]} \quad (6)$$

where $a$ is the radius of the spherical particle, $r$ is the distance from the center of spherical particle ($r \geq a$), $\sigma_r$ is the radial stress, $\sigma_u$ is the circumferential stress, $\nu$ is the Poisson's ratio, $E$ is Young's modulus, $p$ is the pressure at the interface ($p > 0$ during the heating stage), $V$ is the volume fraction and the subscripts p and m represent the particle and the matrix, respectively. The values of interface pressure of Cu/$SiC_p$ composites at all experimental temperature range estimated from Eq. (6) are shown in Table 4, the $SiC_p$ particle is assumed with spherical shape and copper CTE is temperature dependent as shown in Fig. 9.

The difference between $\sigma_{rm}$ and $\sigma_{um}$ is expressed by

$$\sigma = \sigma_{rm} - \sigma_{\theta m} = \frac{p(0.5a^3/r^3 - 2V_p)}{1 - V_p} \quad (7)$$

Plastic deformation can be induced in the matrix at the interface when $\sigma$ exceeds the yield stress of the matrix [18]. In Table 5, it shows the absolute values of $\sigma_r - \sigma_u$ at the interface of Cu/$SiC_p$, only at temperature over certain values the stresses induced at interface are higher than the copper yield stress, i.e. 60 MPa. In the case of lower $SiC_p$ volume fraction, e.g. 35 vol.%, the plastic deformation would not happen in the interface matrix till 400 °C. It also demonstrates clearly that the plastic deformation initiation temperature at interface would decrease as $SiC_p$ volume fraction increases, e.g. interface plastic deformation occurs at temperature as lower as 150 °C for composite with 74 vol.% $SiC_p$.

When differentiating $\sigma$ with particle radius, the following equation can be obtained:

$$\frac{d\sigma}{da} = \frac{1.5pa^3/r^3}{1 - V_p} \quad (8)$$

Eq. (8) demonstrates that $\sigma$ increases with increasing particle size at a defined temperature [19]. Assuming same $SiC_p$ volume fraction, larger $SiC_p$ size would, thus, induced more stress accumulation in the matrix, and more stress releasing would occur during heating and cooling cycle, causing larger strain, i.e. larger CTE value. The experimental data shown in Table 3 complies well with the above ratiocination.

### 3.4. *Influence of particle volume fraction and surface coating on CTE of the composite*

Comparisons of the CTE behaviors of the Cu/$SiC_p$ composite (fabricated with copper coated 25 μm $SiC_p$ under different volume fractions), unreinforced copper P/Med specimen, and commercial casted copper speci-

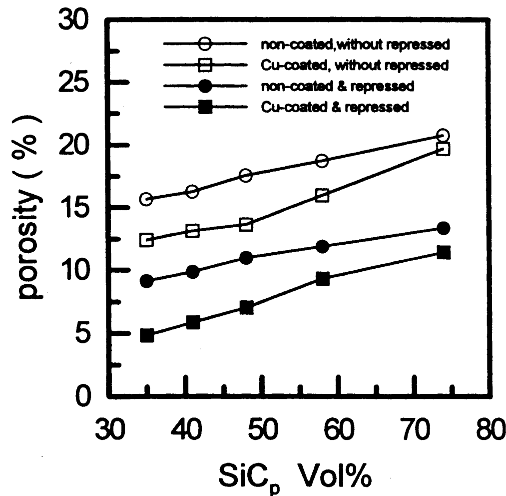


Fig. 7. Porosity as a function of $SiC_p$ vol.% for the composites with 5 μm $SiC_p$ after sintered.

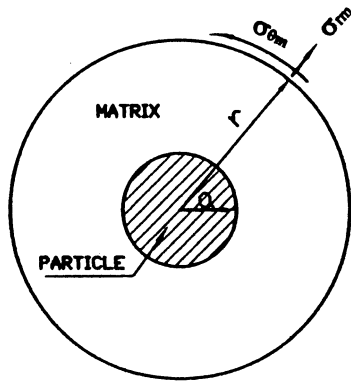


Fig. 8. The model used for thermal stress calculation in particulate composite [16].

men in the temperature range of 50–550 °C for first cycle heating portion are provided in Fig. 9. It can be observed that within the entire temperature range, the addition of high volume fraction $SiC_p$ to copper matrix significantly reduced the CTE of the composite. Such reduction of CTE is reckoned as the results of mixture rule and the intense restriction effect of $SiC_p$ reinforcement on the copper matrix. It is also obvious that the CTE values of composites are lower than those of unreinforced copper specimens fabricated either by P/M or casting method. It was accepted that the CTE values reflected the level of misfit strains introduced in the matrix by the reinforcement [20]. The variation in CTE of the Cu and composite is very distinct at temperatures below 450 °C, which becomes smaller over 450 °C and dwindles to near zero as the temperature rises to 500 °C.

It can be also observed from Fig. 9 that the CTEs of all specimens increased with the increase in temperature, the increasing rate for the specimens in 50–200 °C being much higher than that in 200–550 °C. It is generally known that a considerable amount of internal stress would be released and thermal stress be generated upon heating and cooling processes. During heating process, the thermal stress exhibit as tensile stress on the $SiC_p$ and compressive stress on the copper matrix. On the contrary, during cooling process the thermal residual stresses exhibit as compressive stress on the $SiC_p$ and tensile stress on the copper matrix, and their magnitude may vary with the characteristics of reinforcement and matrix. In the present study, the repress process would undoubtedly introduce a great deal of residual stress in the fabricated specimens. When heating all the specimens in 50–200 °C, most of the residual stress generated during fabrication would be released immediately; resulting in higher CTE increasing rate.

In the absence of phase interaction, the CTE of a composite is always calculated by the simple rule of mixture (ROM) [21]:

Table 3
Instantaneous and mean CTE ( $\times 10^{-6}$ K) of Cu/$SiC_p$ samples

| $SiC_p$ diameter (μm) | $SiC_p$ vol.% | 100 °C | 150 °C | 200 °C | 250 °C | 300 °C | 350 °C | 400 °C | 450 °C | 500 °C | $\overline{CTE}$ (100–500 °C) |
|---|---|---|---|---|---|---|---|---|---|---|---|
| 5 | 35 | 16.5 | 16.2 | 16.8 | 16.1 | 15.7 | 14.9 | 15.8 | 16.4 | 17.2 | 16.2 |
| 5 | 41 | 15.8 | 15.6 | 16.3 | 15.1 | 15.5 | 14.9 | 13.6 | 16.0 | 17.0 | 15.4 |
| 5 | 48 | 15.5 | 15.2 | 15.0 | 14.9 | 14.5 | 14.3 | 14.3 | 13.8 | 14.3 | 14.6 |
| 5 | 58 | 14.7 | 14.9 | 14.5 | 12.6 | 13.2 | 14.0 | 14.2 | 14.9 | 14.0 | 14.1 |
| 5 | 74 | 9.3 | 9.7 | 10.2 | 10.6 | 10.7 | 10.4 | 10.9 | 12.8 | 15.2 | 11.1 |
| 25 | 35 | 12.2 | 13.8 | 14.0 | 14.7 | 15.7 | 16.2 | 17.2 | 17.8 | 18.1 | 17.9 |
| 25 | 41 | 11.2 | 12.9 | 14.0 | 14.7 | 15.3 | 15.8 | 16.3 | 16.8 | 17.3 | 16.8 |
| 25 | 48 | 10.7 | 11.3 | 12.5 | 13.3 | 14.0 | 14.8 | 15.8 | 16.5 | 17.7 | 16.1 |
| 25 | 58 | 9.4 | 10.8 | 12.0 | 13.0 | 14.0 | 14.5 | 15.5 | 16.0 | 17.4 | 15.8 |
| 25 | 74 | 8.0 | 10.4 | 11.0 | 10.8 | 11.4 | 12.1 | 13.1 | 14.1 | 14.8 | 13.9 |
| 47 | 35 | 15.6 | 16.7 | 16.9 | 17.1 | 17.5 | 18.6 | 19.8 | 20.0 | 20.4 | 18.4 |
| 47 | 41 | 13.0 | 16.1 | 17.4 | 14.6 | 16.4 | 18.1 | 18.9 | 18.9 | 19.3 | 17.2 |
| 47 | 48 | 15.0 | 15.8 | 16.0 | 16.7 | 16.3 | 17.0 | 18.1 | 18.3 | 19.5 | 17.1 |
| 47 | 58 | 13.5 | 16.4 | 16.6 | 16.2 | 16.0 | 16.9 | 17.1 | 16.4 | 17.4 | 16.4 |
| 47 | 74 | 11.2 | 12.5 | 12.7 | 12.5 | 15.0 | 18.9 | 16.7 | 16.4 | 19.1 | 15.3 |

Table 4
Pressure at the interface of composite (unit: MPa)

| $SiC_p$ vol.% | 100 °C | 150 °C | 200 °C | 250 °C | 300 °C | 350 °C | 400 °C | 450 °C | 500 °C | 550 °C |
|---|---|---|---|---|---|---|---|---|---|---|
| 35 | 26.2 | 53.3 | 82.4 | 112.1 | 142.4 | 173.6 | 205.5 | 238.6 | 272.8 | 338.6 |
| 41 | 23.9 | 49.1 | 75.3 | 102.3 | 130.0 | 158.5 | 187.6 | 217.8 | 249.1 | 299.1 |
| 48 | 21.2 | 43.6 | 66.8 | 90.8 | 115.4 | 140.7 | 166.6 | 193.4 | 221.1 | 274.5 |
| 58 | 17.4 | 35.7 | 54.8 | 74.5 | 94.6 | 115.4 | 136.6 | 158.6 | 181.3 | 225.0 |
| 74 | 10.9 | 22.5 | 34.5 | 46.9 | 59.6 | 72.6 | 86.0 | 99.9 | 114.2 | 141.7 |

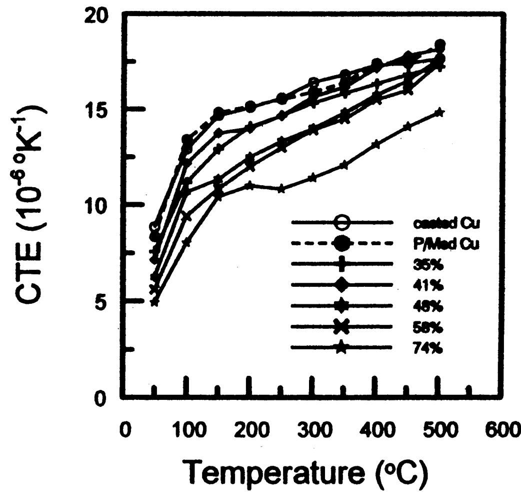


Fig. 9. Comparison of CTE behaviors of Cu/$SiC_p$ composites with 25 μm $SiC_p$ in different particle volume percents.

$$\alpha_c = \alpha_m V_m + \alpha_p V_p \quad (9)$$

where $\alpha$ is CTE, $V$ is the volume fraction, and the subscripts c, m, and p refer to the composite, matrix and particle, respectively. The ROM model is often considered inappropriate because it does not take account of the microstructure and strain interaction.

However, it is known that micro stress often exists between the phases, and these stresses influence the thermal expansion behavior of the composite body. Several researchers have given expressions for the CTE of the particulate composites taking into account the stress interaction between phases. According to Turner's model [22], the CTE of a particular composite is given by:

$$\alpha_c = \frac{\alpha_m V_m K_m + \alpha_p V_p K_p}{V_m K_m + V_p K_p} \quad (10)$$

where $K$ is the bulk modulus.

Turner's model is based on the assumption that only uniform hydrostatic stresses exist in the phases. Another model for particulate composites is given by Kerner [23], which accounts for both shear and isostatic stresses developed in the component phases, and gives the CTE for the composite as:

$$\alpha_c = \alpha_m - (\alpha_m - \alpha_p) \times \frac{K_p(3K_m + 4G_m)V_p}{K_m(3K_p + 4G_m) + 4(K_p - K_m)G_m V_p} \quad (11)$$

where $G$ is the shear modulus.

A comparison of the experimental and theoretical CTE values obtained by using these three models is presented in Fig. 10. In the calculation of the predictions of the models, the CTE data for copper and SiC are taken from commercial specimens measured at 100 °C ($\alpha_{SiC} = 5.32 \times 10^{-6}$ $K^{-1}$, $\alpha_{Cu} = 16.15 \times 10^{-6}$ $K^{-1}$), the bulk modulus of SiC is taken as 450 GPa. The $K_m$ and $G_m$ values of matrix, influenced by compact fractional porosity, must be concerned. As reported by Lally et al. [24], both the yield and ultimate strengths of compacts could be improved by high compact densities. It means that the yield and ultimate strengths decreased with increasing porosity. Several researches [25–27] are also focused on the relationship between the density and the strength of sintered metal components. All of them reached the same conclusion, that is, the ultimate tensile strength of a powder compact decreased with increasing fractional porosity. The dependence of Poisson's ratio of powder compact on pore volume fraction is given as [28]:

Table 5
$|\sigma_r - \sigma_0|$ value at the interface of composite (unit: MPa)

| $SiC_p$ vol.% | 100 °C | 150 °C | 200 °C | 250 °C | 300 °C | 350 °C | 400 °C | 450 °C | 500 °C | 550 °C |
|---|---|---|---|---|---|---|---|---|---|---|
| 35 | 8 | 16 | 25 | 34 | 44 | 53 | 63 | 73 | 84 | 104 |
| 41 | 12 | 26 | 41 | 55 | 71 | 86 | 102 | 118 | 135 | 168 |
| 48 | 18 | 38 | 59 | 80 | 102 | 125 | 147 | 171 | 196 | 243 |
| 58 | 27 | 56 | 86 | 117 | 149 | 181 | 215 | 249 | 285 | 354 |
| 74 | 41 | 84 | 130 | 177 | 225 | 274 | 324 | 377 | 430 | 534 |

$$\nu_m = \nu(1 - p_f)^a \quad (12)$$

where $\nu$ is the Poisson's ratio of matrix, the exponent $a$ ranges from 1.92 for cold forging to 2.00 for hot forging (1.92 was used in this study for calculating Turner's and Kerner's model values).It is shown in Eq. (12), that the Poisson's ratio would decrease with increasing fractional porosity.

It is known that the bulk modulus of matrix ($K_m$) is given as

$$K_m = \frac{E}{3(1 - 2\nu_m)} \quad (13)$$

and the shear modulus of matrix ($G_m$) is given as

$$G_m = \frac{E}{2(1 + \nu_m)} \quad (14)$$

Eqs. (12) and (13) show that the bulk modulus of matrix would decrease with increasing fractional porosity; on the contrary, Eqs. (12) and (14) show that the shear modulus of matrix would increase with increasing fractional porosity. Taking account of Eqs. (12)–(14) into Eq. (11), the relationship of composite CTE as functions of fractional porosity and $SiC_p$ volume fraction is calculated and shown in Fig. 11. It is observed from the figure that for pure copper, i.e. 0 vol.% $SiC_p$, porosity has little effect on CTE. As $SiC_p$ volume fraction increase, the CTE tends to decrease linearly with increase of porosity. However, until about 80% $SiC_p$ vol.%, the above tendency diminished gradually, i.e. the porosity exerts only negligible effect on CTE.

Fig. 10 also shows that the CTE values of coated composites are lower than those of non-coated $SiC_p$ composites, this mainly stems from the fact that in the former copper has undergone plastic flow during the heating process, and the plastic flow was retarded by the well bonded $SiC_p$. For those with non-coated $SiC_p$ composites, bad bonding between Cu matrix and $SiC_p$ makes the major thermal expansion of composite being contributed by copper matrix; therefore, the CTE of composites approach the CTE of copper.

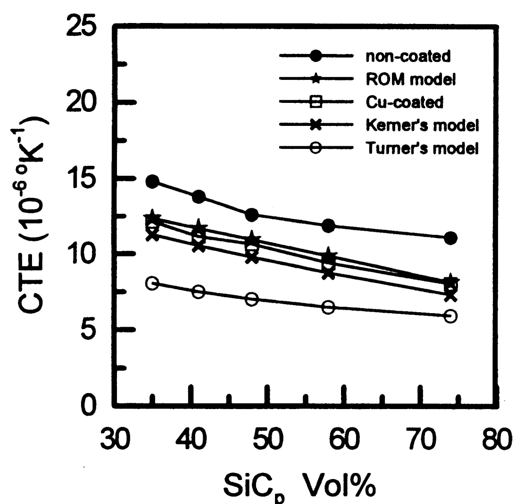


Fig. 10. Comparison of experimental and theoretical values of CTE for different particulate composites (temperature: 100 °C, $SiC_p$ particle size: 25 μm, $\alpha_{SiC} = 5.32$ ppm, $\alpha_{Cu} = 16.15$ ppm).

Sun et al. [29] reported that the experimental CTEs of particulate composites are often found lying between the predictions of Turner's and Kerner's models. However, in Fig. 10, the experimental values approach most closely the values estimated by ROM model, and agree better with Kerner's model as compared with Turner's model. This trend is not unexpected since the P/Med composites have more pores than those made by the casting method that could obtain higher density. Both Kerner's and Turner's models would give descended CTE values if the porosity was introduced to Eqs. (11) and (12) for calculating $K_m$ and $G_m$ values.

### 3.5. The thermal hysteresis behavior of the composite

The measured thermal linear expansion curves of different $Cu/SiC_p$ composites, as a function of temperature, are presented in Fig. 12. The CTE values for the individual composites have been given in Table 3. As shown in Fig. 12, the percent linear change (PLC) versus temperature curves of different $Cu/SiC_p$ composites show similar characteristics, i.e. after a complete heating and cooling cycle, the composite retain ca 0.1–0.3% positive residual strain, and with increasing $SiC_p$ volume fraction, the PLC of the 5 μm sample decreased, the PLC of 25 μm sample converged to approximately 0.22%, while that of 47 μm diverged in a complex way. The thermal hysteresis behavior can be explained in terms of the weak interface between reinforcements and matrix or large internal stress released in the composites. Once the composite had undergone significant plastic deformation during the heating process, the lack of bonding force could not produce large enough stress to deform the matrix back to its original size upon cooling.

As shown in Fig. 12, the 5 μm $SiC_p/Cu$ composites, with exception of 35 vol.% sample, showed a relatively smaller hysteresis values upon cooling as compared with that of the 25 μm $SiC_p/Cu$. This result can be stemmed from that larger thermal hysteresis would be induced while higher stress inherent in matrix was obtained when larger $SiC_p$ size composites were repressed using same operating procedure. However, the hysteresis of 47 μm $SiC_p/Cu$ are more diversified than others, more pores in this composite and/or the possibly bonding deterioration, as larger thermal stress induced with larger particle size (derived from Table 2), are reckoned as the possible reasons. Since the thermal hysteresis behavior of a material could be a problem in a real application, the thermal cycling test was carried out on composites and commercial copper bar in order to determine if the thermal hysteresis were matrix related. Fig. 13 shows the

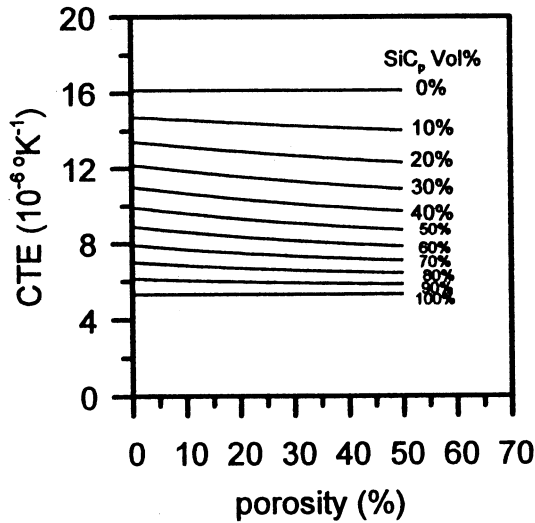


Fig. 11. The relationship of CTE, fractional porosity and $SiC_p$ volume fraction of composite

thermal linear expansion curves for the 25 μm, 48 vol.% $SiC_p$/Cu sample obtained from four continuous thermal cycles, and it can be found that the thermal hysteresis behavior is observed in all thermal cycles. In each subsequent thermal cycles, the thermal hysteresis behavior is gradually lessened. This probably can be ascribed to that the internal residual stress accumulated in the repressing process is released gradually at each thermal cycle. Besides, at the high temperature portion of each cycle, like that at 550 °C, the specimens still have some residual stress in the first heating cycle which was gradually dissipated at each subsequent heating and cooling cycle. In other words, the thermal expansion behavior of composite is thermal history dependent, thus, the CTE data are also dependent on the thermal history.

The thermal expansion behavior of a copper sample cut from a commercial copper bar was measured with three thermal cycles and the results are given in Fig. 14. The thermal hysteresis behavior can also be observed during the first thermal cycle, and is removed from the sample during the subsequent thermal cycles. It shows that the specimen was stress-free at 550 °C. Comparing with Fig. 13, the hysteresis strain of the commercial copper bar after the thermal cycle was found to be much smaller than that for the Cu/$SiC_p$ composite, this indicated that lower internal residual stress is inherent in copper bar than in composites.

High defect density and residual stresses in the composites made by powder metallurgy could be the reasons for the hysteresis behavior observed herein. During the heating stage of thermal cycle, tensile stress is developed on $SiC_p$ and compressive stress on copper matrix, this is caused by larger Cu expansion than that of $SiC_p$ reinforcement in the case that $SiC_p$ and Cu are under well bonding status. It is obvious that the

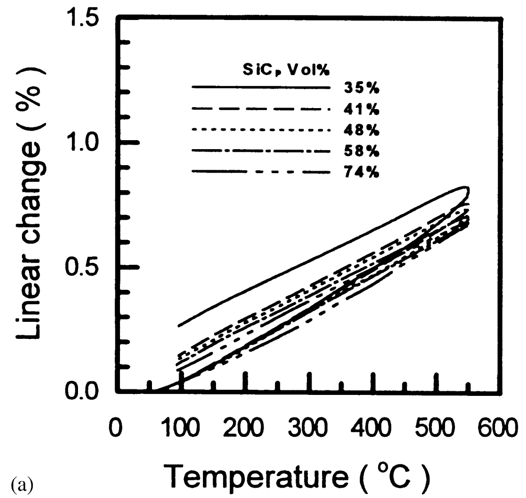


(a)

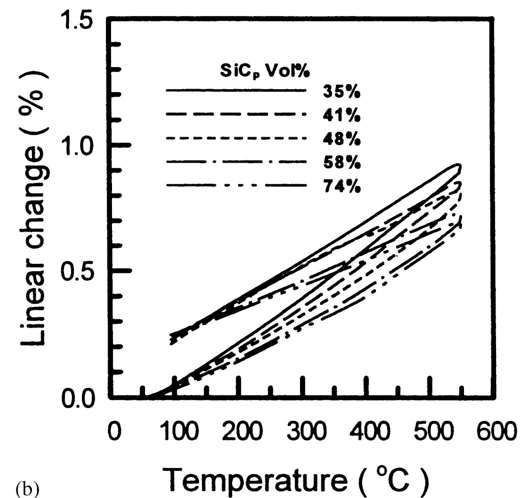


(b)

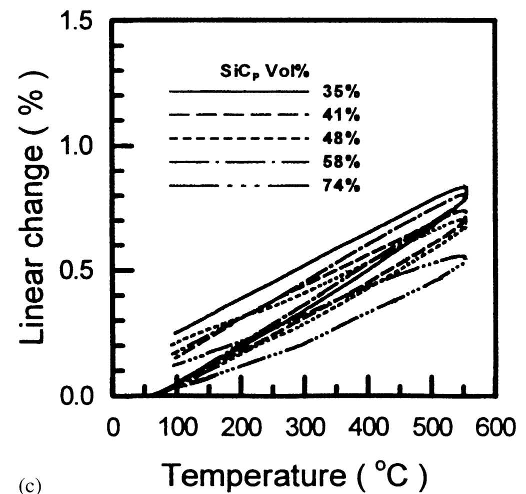


(c)

Fig. 12. Thermal linear expansion curves for Cu/$SiC_p$ composites for a heating and cooling cycle with different particle sizes: (a) 5 um, (b) 25 um and (c) 47 um.

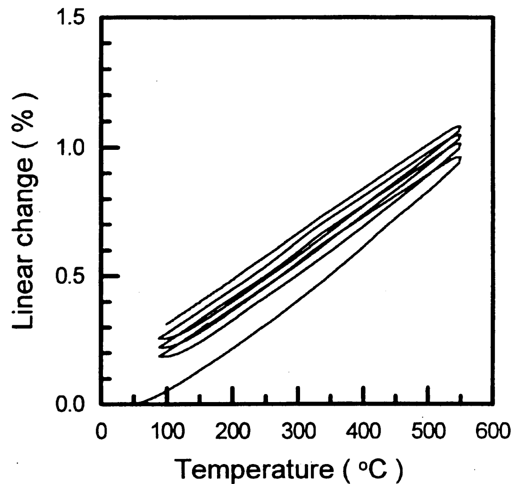


Fig. 13. Thermal linear expansion curves for the 25 μm, 48 vol.% $SiC_p$/Cu sample corresponding to four continuous thermal cycles.

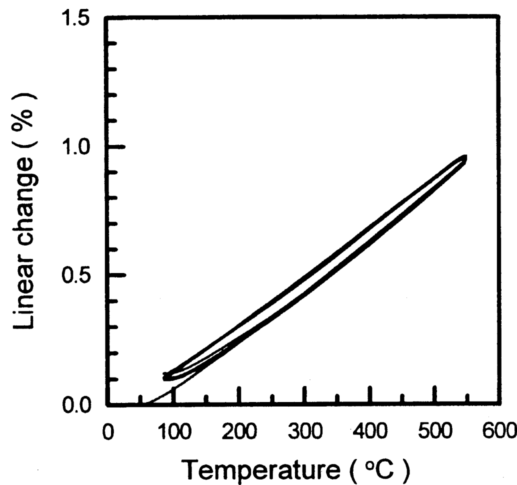


Fig. 14. Thermal linear expansion curves for a commercial copper bar from three continuous thermal cycles.

composite CTE would be lower than the values calculated by rule of mixture, and the experimental values of non-coated specimen, these phenomena are proved in Fig. 10. On the contrary, during the cooling stage of thermal cycle, the thermal residual stresses might affect the overall CTE of the Cu/$SiC_p$ composite in two ways. The tensile portion upon the matrix could enlarge the distance of the Cu atom and thus reduce the expansion ability of the matrix. Meanwhile, the compressive stresses on the reinforcement would enhance the restriction effect of $SiC_p$ on the matrix and also lessen CTE of the Cu/$SiC_p$ composite. The cooling portion curves shown in Fig. 12 show lower slope than the heating portion curves, i.e. the CTE values during heating stage are larger than that during cooling stage, can be an apparent proof of the above ratiocination. If the difference of stress among heating and cooling stage is large, i.e. more residual stress is released in the composite, larger hystersis would be observed. In Cu bar specimen, with smaller residual stress after first cycle and nil matrix/reinforcement interaction, same thermal cycling behavior is expected as shown in Fig. 14.

## 4. Conclusions

The thermal expansion behavior of Cu/$SiC_p$ composite fabricated by powder metallurgy method, with different $SiC_p$ volume fraction and surface coating, was studied in this paper in the temperature range of 50–550 °C, and the following conclusions have been drawn.

A completely continuous copper film on silicon carbide particle can be obtained by electroless plating process to promote bonding between Cu and $SiC_p$. The Cu/$SiC_p$ composites prepared by the powder metallurgy method show a uniform microstructure in which silicon carbide particles are distributed evenly in the copper matrix.

The MMC CTE could be decreased effectively through well bonding between reinforcement phase and metal matrix.

The CTE and thermal hysteresis strain generally increases with increasing $SiC_p$ particle size. The composites exhibited positive thermal strain when cooled down from the peak temperature to room temperature, which can be explained in terms of the residual stresses and the interfacial bonding between copper and silicon carbide. The magnitude of this thermal strain is a function of $SiC_p$ volume fraction and number of thermal cycles.

## References

[1] B. Ogel, R. Gurbuz, Mater. Sci. Eng. A301 (2001) 213.
[2] B.G. Kim, S.L. Dong, S.D. Park, Mater. Chem. Phys. 72 (2001) 42.
[3] G. Manchang, K.S. Bong, J. Mater. Lett. 46 (5) (2000) 296.
[4] K. Biswas, G.S. Upadhvy, Mater. Des. 9 (5) (1998) 231.
[5] Y.L. Shen, Mater. Sci. Eng. A152 (1998) 269.
[6] S.G. Konsowski, A.R. Helland, Electronic Packaging of High Speed Circuitry, McGraw-Hill, New York, 1997, p. 60.
[7] H. Ledbetter, M. Austin, Int. J. Thermophys. 12 (1991) 731.
[8] K. Parasan, S. Palaniappan, S. Seshan, Composite 28 (1997) 1019.
[9] K. Premkumar, M.H. Hunt, P.R. Sawtell, J. Met. 44 (1992) 24.
[10] P. Yih, D.D.L. Chung, J. Mater. Sci. 31 (1996) 399.
[11] Y.L. Shen, M. Finot, A. Needleman, S. Suresh, Acta Metall. Mater. 39 (1991) 735.
[12] P. Yih, D.D.L. Chung, J. Mater. Sci. 34 (1999) 359.
[13] F.P. Beer, E.R. Johnston, Mechanical Behavior of Materials, second ed., McGraw-Hill, New York, 1996, p. 806.
[14] T.H. Courtney, Mechanical of Materials, McGraw-Hill, New York, 1996, p. 46.
[15] D. Masutti, J.P. Lentzs, F. Delanny, J. Mater. Sci. Lett. 9 (1990) 340.

[16] D. Brooksbank, K.W. Andrews, J. Iron Steel Inst. 208 (1970) 582.
[17] R.U. Vaidya, K.K. Chawla, Comp. Sci. Technol. 50 (1994) 13.
[18] K.K. Chawla, Metallography 6 (1973) 155.
[19] Y.Z. Wan, Y.L. Wang, H.L. Luo, X.H. Dong, G.X. Cheng, J. Mater. Sci. Lett. 18 (1999) 1059.
[20] Y. Takao, M. Taya, J. Appl. Mech. 52 (1985) 806.
[21] ASM Handbook, vol. 2, American Society for Metals, Metals Park, OH, 1991, p. 401.
[22] P.S. Turner, J. Res. NBS 37 (1946) 239.
[23] E.H. Kerner, Proc. Phys. Soc. 69 (1956) 808.
[24] F.T. Lally, I.J. Toth, J. Dibenedetto, Forging of Steel Powder Products, Metal Powder Industries Federation, Princeton, NJ, 1973, p. 103.
[25] A. Salk, V. Miskovic, E. Dudrova, E. Rudnayova, Powder Metall. Int. 6 (1974) 128.
[26] N.A. Fleck, R.A. Smith, Powder Metall. 24 (1981) 121.
[27] V.T. Troshchenko, Soviet Powder Metall. Metal Ceram. 2 (1963) 179.
[28] R.M. German, Powder Metallurgy Science, second ed., Metal Powder Industries Federation, Princeton, NJ, 1994, p. 323.
[29] Q. Sun, O.T. Inal, Mater. Sci. Eng. B41 (1996) 261.